analytical chemistry

Article

pubs.acs.org/ac

Recessed Ring–Disk Nanoelectrode Arrays Integrated in Nanofluidic Structures for Selective Electrochemical Detection

Chaoxiong Ma,[†] Nicholas M. Contento,[‡] Larry R. Gibson, II,[‡] and Paul W. Bohn*[,†,‡]

[†]Department of Chemistry and Biochemistry, and [‡]Department of Chemical and Biomolecular Engineering, University of Notre Dame, Notre Dame, Indiana 46556, United States

ABSTRACT: Arrays of recessed ring–disk (RRD) electrodes with nanoscale spacing fabricated by multilayer deposition, nanosphere lithography, and multistep reactive ion etching were incorporated into nanofluidic channels. These arrays, which characteristically exhibit redox cycling leading to current amplification during cyclic voltammetry, can selectively analyze electroactive species based on differences in redox reversibility, redox potential, or both. Using $Ru(NH_3)_6^{3+}$ and ascorbic acid (AA) as model reversible and irreversible redox species, the selectivity for electrochemical measurement of $Ru(NH_3)_6^{3+}$ against a background of AA improves from ~10, for an array operated in a fluidically unconstrained geometry, to ~70 for an array integrated within nanofluidic channels. RRD arrays were also used for the detection of dopamine in the presence of AA by cyclic voltammetry. A linear response ranging from 100 nM to 1 mM with a detection limit of 20 nM was obtained for dopamine alone without nanofluidic confinement. In nanochannel-confined arrays, AA was depleted by holding the ring electrodes at +0.5 V versus Ag/AgCl, allowing interference-free determination of dopamine at the disk electrodes in the presence of a 100-fold excess of AA. For selective detection of electrochemically reversible interfering species on an RRD array without nanochannel confinement, a ring potential can be chosen such that one species exhibits exclusively cathodic (anodic) current, allowing the other species to be determined from its anodic (cathodic) current. This approach for selective detection is demonstrated in a mixture of $Ru(NH_3)_6^{3+}$ and $Fe(CN)_6^{3-}$, which have resolved redox potentials. The same principle was successfully applied to differentiate species with overlapping redox potentials, such as dopamine/$Fe(CN)_6^{3-}$ and ferrocenemethanol/$Fe(CN)_6^{4-}$.

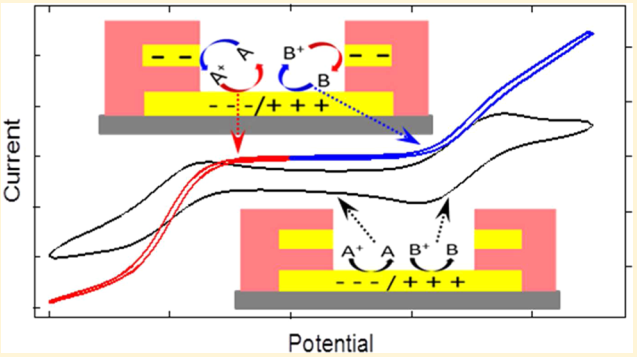

Microfluidic chip-based devices are advancing rapidly with the aim of providing portable and low-cost sensing for chemical[1−3] and biochemical analysis.[4−9] Furthermore, recent advances in nanofabrication capabilities have enabled the fabrication of precisely controlled nanoscale fluidic devices.[1,3,10−13] Incorporation of robust sensing modules within these fluidic systems is highly desirable for developing compact sensors which may replace traditional detection techniques, such as mass spectrometry[14−16] and fluorescence spectroscopy,[2,17,18] at least in some applications. Electrochemical detection is a promising approach, because it is sensitive, compatible with micro/nanofluidic systems, and inexpensive.[10,19−21] For instance, metal film microelectrodes deposited on glass substrates can be easily integrated within poly(dimethylsiloxane) (PDMS) microchannels.[1,17,22] The resulting devices provide rapid, label-free measurements, with currents that are directly proportional to the concentration of the electroactive species.

In practice, microelectrodes are typically used, because they exhibit fast response times, low charging currents, and stable steady-state responses.[23−25] In addition, the reduced electrode size allows multiple elements to be incorporated within the small sensing area, thus enabling multiplexed and parallel analysis. However, microelectrodes in confined geometries, such as microchannels, produce relatively small currents, a direct consequence of the limited diffusional boundary layer arising from the channel geometry.[12,13,26] In addition, steady-state responses can deteriorate, because the diffusion region reaches the boundary of the channel before radial diffusion is developed.[1,12,26] External pumps[27,28] can be used for convective delivery of electrochemical reagents in microfluidic systems; however, this compromises miniaturization and portability. Improved sensitivity has also been achieved by coupling electrochemistry with electrophoresis[10,22] or electroosmotic flow[29−31] to enhance mass transport of analytes to the sensing electrodes. This strategy works well in a range of applications, but potential interference of the electric field used to drive electrokinetic flow usually requires a decoupling strategy.[10,22,31]

Redox cycling[3,12,13,26,32,33] (RC) offers a compelling alternative to enhance currents from electrochemical measurements within micro- or nanochannels. The RC effect usually occurs between two closely spaced electrodes operated in generator–collector (GC) mode,[32,33] in which one is held at a sufficiently positive potential to oxidize the analyte and the

Received: August 1, 2013
Accepted: September 6, 2013
Published: September 6, 2013

other is held at (or swept to) a reducing potential. The electrode geometry allows the species generated at one electrode to be collected by the other electrode, since the diffusion zones overlap. As a result, the redox couple can be cycled between the two electrodes, amplifying the current in proportion to the average number of redox cycles. In addition, a steady-state voltammetric response[3,32] can be obtained in cyclic voltammetry (CV) measurements, because the number of molecules reaching the electrode surface is not governed by the diffusion boundary.

Beyond providing steady-state responses with enhanced sensitivity, the RC effect can also be exploited to improve the selectivity of electrochemical measurements.[12,34−36] It is especially important to address the low specificity of electrochemical detection in applications not coupled to molecular separations, because target analytes in biological or environmental samples can be overwhelmed by intrinsic interferences.[4,19,22,36,37] The RC effect requires species to be redox reversible; accordingly, irreversible species are not regenerated for cycling and produce no RC or current amplification, thus affording a strategy for enhancing selectivity.[12,13,37] In addition, the irreversible interfering species can also be depleted at the generator electrode,[12,37] enabling determination of reversible analytes at the collector electrode. On the other hand, to differentiate two species with similar redox reversibility and potential, the potential of the generator electrode can be adjusted such that one species exhibits a cathodic response while the other exhibits an anodic response on the collector electrodes.[36,37]

To take advantage of the RC effect for sensitive and selective measurements, electrodes with different geometries such as interdigitated electrode arrays,[13,26,32,35−39] thin-layer cells,[12,40] and ring/plane recessed disk electrode arrays[33,37] have been fabricated. The strong dependence of the RC effect and the resulting current amplification on the interelectrode distance requires the fabrication of the device to include nanoscale features for enhanced performance.[12,32,40] Recently, we have developed a robust procedure for the fabrication of arrays of recessed ring−disk (RRD) electrodes, with both size and spacing in the nanoscale range, by combining layer-by-layer deposition, nanosphere lithography (NSL), and a multistep reactive ion etching (RIE) process.[3] Such RRD arrays showed 10× current amplification in an open geometry and 50× when integrated in a nanochannel.[3]

In this study, RRD arrays are used for selective determination of electrochemically active analytes in the presence of both irreversible and reversible interferences. As one example, detection of dopamine (DA) from biological samples remains challenging due to its relatively low basal concentration and the presence of interfering substances.[4,19,34,40−43] Ascorbic acid (AA)[42,44] represents one such interference that is particularly troublesome, because it has a similar oxidation potential but is present at several orders of magnitude higher concentration than DA. Because AA is an irreversible redox species,[12,37,40] it is possible to minimize the interference of AA using the RC effect.

To explore these selectivity enhancements, a systematic study of analyte/interference redox systems with different properties was undertaken. First, the selectivity of nanoscale RRD arrays with and without nanochannel confinement was evaluated using a mixture of $Ru(NH_3)_6^{3+}$ and AA. Next, in order to test detection sensitivity of the RRD array, CV measurements of different concentrations of DA were conducted to determine the linear response range and the limit of detection (LOD) on the array in open geometry. To take advantage of the nanochannel confinement for selective measurement, ring electrodes were held at 0.5 V to deplete AA and eliminate its interference during DA detection. Interference-free detection of DA in the presence of a 100-fold excess of AA was achieved in the nanochannel configuration.

Next, the selective detection of analytes with similar reversibility, but different redox potential, was explored on RRD arrays without nanochannel confinement. In this case, channel confinement was not employed, because it does not significantly affect the current amplification of the reversible species or further improve measurement selectivity. In these measurements, an appropriate generator potential was chosen such that one species exhibits a cathodic current, while the other exhibits only an anodic current on the collector.[36,37,45,46] The selectivity obtained using this strategy depends strongly on the amplification factor and conversion efficiency of the electrode geometry. The capabilities of the RRD arrays were evaluated using analytes with redox potentials ranging from completely separated ($Ru(NH_3)_6^{3+}/Fe(CN)_6^{3-}$), to modestly overlapping (dopamine/$Fe(CN)_6^{3-}$), to heavily overlapping (ferrocenemethanol/$Fe(CN)_6^{4-}$). Interfering species of 5-fold higher concentration result in less than 10% deviation of the limiting current of the target analyte, even when redox potentials are heavily overlapping.

EXPERIMENTAL SECTION

Reagents and Materials. All chemicals were used as received, including hexaammineruthenium(III) chloride ($Ru(NH_3)_6Cl_3$), ascorbic acid, dopamine hydrochloride, potassium ferricyanide ($K_3Fe(CN)_6$), potassium ferrocyanide ($K_4Fe(CN)_6$), ferrocenemethanol, potassium chloride, sulfuric acid (95%), hydrogen peroxide (30%), ethanol, acetone, and chloroform, all obtained from Sigma-Aldrich. Photoresist AZ5214E (AZ Electronic Materials) and PDMS (Dow Corning) were used following manufacturers' procedures. Chromium chips (Alfa Aesar) and gold coins (Canadian Gold Maple Leaf) were used as metal sources for thermal deposition. Solutions of underivatized polystyrene spheres (0.92 μm in diameter, 0.25 wt %, Corpuscular Inc.) were diluted 1:1 (v/v) with ethanol prior to use. All solutions for electrochemical measurements were prepared using deionized (DI) water ($\rho \sim 18$ MΩ cm) generated from a Milli-Q Gradient water purification system (Millipore, Bedford, MA).

Device Fabrication. Nanoscale RRD arrays were fabricated following a previously developed procedure.[3] As illustrated in Figure 1a, the RRD arrays were fabricated via layer-by-layer deposition of $Au/SiN_x/Au/SiO_2$, nanosphere lithography, followed by a multistep RIE process. Parts b and c of Figure 1 show a schematic diagram and a scanning electron microscopy (SEM) image of a fabricated array containing cylindrical nanopores of ∼650 nm diameter with ∼1.0 μm pitch. The thickness of SiO_2, SiN_x, and both Au layers are all 200 nm. The number of RRD electrodes in an array can be calculated from the array size and the pore density (∼1 pore μm^{-2}). For example, an array of 25 μm × 100 μm contains ∼2500 RRD electrodes. The RRD arrays can be used for electrochemical characterization directly in an open geometry or after integration with nanochannels, depending on the goal of the measurement. To integrate the RRD arrays with nanofluidic delivery architectures, five channels of SiN_x were constructed on top of the arrays. Substrates with arrays obtained above were coated with an additional 300 mn layer of

dx.doi.org/10.1021/ac402417w | Anal. Chem. 2013, 85, 9882−9888

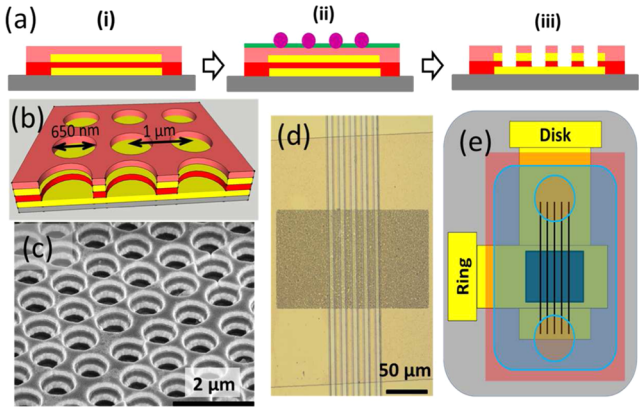

Figure 1. (a) Schematic cross section showing the fabrication procedure for the RRD array, including (i) layer-by-layer deposition, (ii) nanosphere lithography, and (iii) multistep reactive ion etching. The colors represent different layers: gray (glass slide), yellow (Au), red (SiN_x), pink (SiO_2), purple (polystyrene spheres), and green (Cr). (b) Schematic diagram of the ring−disk geometry of the array. (c) An SEM image of the array at 50° tilt. (d) An optical image of the array integrated with SiN_x channels. (e) Schematic diagram of the macroscopic layout of the RRD array (dark blue) integrated with channels (black) and covered by a piece of PDMS (light blue) with two circular wells.

SiN_x, patterned by photolithography, and etched by RIE. Each nanochannel measured 300 nm deep, 5 mm long, and 5 μm wide, with 10 μm separation between nanochannels (Figure 1d). The resulting channels were then sealed with a piece of PDMS with two wells separated by ∼5 mm using oxygen plasma treatment, Figure 1e.[47]

Electrochemical Characterization. For the electrochemical measurement in open geometry, ∼30 μL of solution was added to a PDMS well with diameter of 3 mm covering the array. In the confined geometry, the nanochannels were filled with solution (∼100 μL) under vacuum after being sealed with a PDMS top layer. Cyclic voltammetry experiments were conducted on a CHI bipotentiostat (842c, CH Instruments Inc.) using a Pt wire and a Ag/AgCl electrode, respectively, as auxiliary and reference electrodes, which were both immersed in the solution volume defined by the PDMS wells. Reproducible solution filling, indicated by CV responses with <5% variation across seven replicate runs (data not shown), was achieved owing to the hydrophilic nature of the surface after RIE processing. In all measurements, the potential of the disk electrodes was swept, and the ring electrodes were held at a constant potential (GC mode) or disconnected (non-GC mode). Phosphate buffer (pH 7) consisting of 0.5 M phosphate and 0.5 M KCl was used for measurements in solutions of dopamine and/or ascorbic acid. Sulfuric acid (2.0 M) was used to adjust the pH of the solution to pH 2 for the analysis of dopamine in the presence of $Fe(CN)_6^{3-}$. Unless otherwise specified all potentials quoted here are taken versus a macroscopic Ag/AgCl reference electrode.

RESULTS AND DISCUSSION

Selective Detection of $Ru(NH_3)_6^{3+}$ in the Presence of Ascorbic Acid: Nanochannel Effect. One important property of the nanochannel-confined RRD array is that current amplification of the reversible species due to redox cycling is not diminished by nanochannel confinement. This property is useful to selectively measure species with differing degrees of redox reversibility, as evaluated using a mixture of $Ru(NH_3)_6^{3+}$ and AA. Figure 2 shows the CV results on the array with and without nanochannel confinement in both GC and non-GC mode.

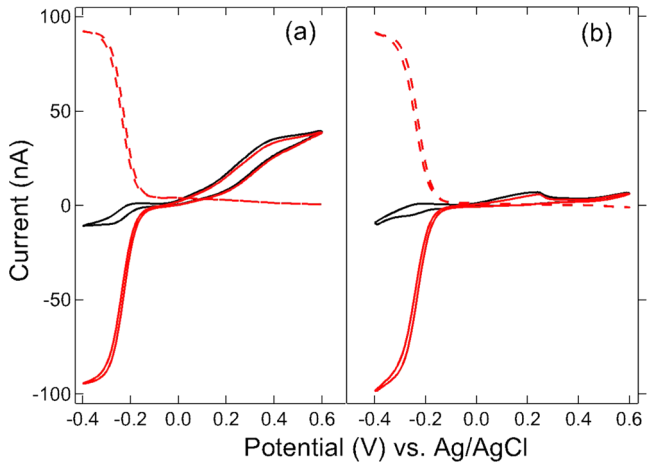

Figure 2. Cyclic voltammograms measured in a mixture of 1 mM $Ru(NH_3)_6^{3+}$ and 5 mM ascorbic acid using (a) an unconfined 25 μm × 100 μm RRD array and (b) an array of the same size integrated with nanochannels. Disk electrodes are swept at 100 mV/s. Ring electrodes are disconnected (black, non-GC mode) or held at 0.0 V vs Ag/AgCl (red, GC mode). Disk current (solid) and ring current (dashed).

In the open geometry, i.e., when there is no nanochannel delivery to the RRD array, Figure 2a shows that running the CV in GC mode produces ∼10× larger limiting current for the reduction of $Ru(NH_3)_6^{3+}$ (solid red curve, Figure 2a) compared to non-GC mode (solid black curve). In contrast, the oxidation of AA, which begins anodic of 0.0 V, shows no obvious difference in limiting current between GC and non-GC mode. This observation can be attributed to its redox irreversibility, which is further confirmed by the absence of a cathodic current for AA on the ring electrodes. In contrast, Figure 2b, obtained in a nanochannel-confined geometry, shows the same enhancement of $Ru(NH_3)_6^{3+}$ when the CV is obtained in GC mode, with the ring electrode held at 0.0 V, but the anodic wave associated with AA oxidation is greatly diminished.

The interaction of the diffusional boundary layer with the physical boundaries of the nanochannels is plainly seen in the decreased limiting current of the in-channel CV measurement on the integrated electrode operated in non-GC mode. This effect is observed for both $Ru(NH_3)_6^{3+}$ and AA, with the limiting current in non-GC mode ∼80% smaller in the nanochannel-confined geometry than in the open geometry. On the other hand, the limiting current of $Ru(NH_3)_6^{3+}$ reduction (disk) or $Ru(NH_3)_6^{2+}$ oxidation (ring) in GC mode is similar whether the electrodes are coupled with channels or not, since $Ru(NH_3)_6^{3+/2+}$ principally diffuses between ring and disk electrodes and is thus not affected by the channel walls. In the nanochannel-confined geometry, AA exhibits no cathodic current on the ring electrodes, similar to the open geometry, and its peak currents are nearly identical in GC and non-GC mode.

The dependence of the CV of $Ru(NH_3)_6^{3+}$ and AA on both electrode geometry and GC/non-GC operation mode demonstrates a range of strategies to achieve selective detection in the presence of a redox-irreversible interference. After normalizing to the relevant concentration, the limiting currents shown in

dx.doi.org/10.1021/ac402417w | Anal. Chem. 2013, 85, 9882−9888

Figure 2 show that the selectivity of the $Ru(NH_3)_6^{3+}$ to AA operated in GC mode is ~10 when the RRD array is operated in bulk solution (unconfined) and ~70 when confined in a nanochannel. This improvement in selectivity when nanochannel confinement is used in conjunction with redox cycling arises principally from the interaction of the diffusional boundary layer with the physical walls of the nanochannel.

Linear Response and Limit of Detection of Dopamine. In order to quantitatively assess the performance of the RRD arrays, DA was detected by cyclic voltammetry in GC mode. The potential of the disk electrodes was scanned, while holding the ring electrodes at 0.0 V, and the ring electrode limiting current exhibited a linear dependence on DA concentration over 4 orders of magnitude, as shown in Figure 3. In these

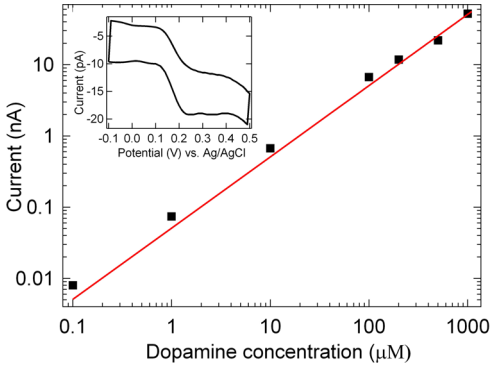

Figure 3. Limiting current at ring electrodes as a function of dopamine concentration (points) and a linear fit (line). Voltammograms were measured on a 25 μm × 50 μm RRD array by scanning the disk electrodes at 10 mV/s and holding the ring electrodes at 0.0 V. Inset: ring current measured in 0.1 μM dopamine while the disk potential was scanned.

experiments, the ring current is used as the analytical signal, because it exhibits a smaller charging current than the disk. An LOD of 20 nM was obtained for DA on a 25 μm × 50 μm RRD array with 200 nm electrode separation. The LOD depends strongly on the current amplification, which in turn depends on the specific geometry of the RRD array, which determines the maximum current measurable in the CV. A higher amplification factor can be achieved by using a thinner insulating layer; however, this also results in increased charging current at the ring electrodes due to charge leakage, a problem that is especially noticeable with SiN_x layers <200 nm thick. On the other hand, using a larger RRD array area to increase the measurable current by increasing the number of recessed ring−disk pairs contributing to the signal can result in larger background currents. Alternatively, engineering the insulating layer to provide better electrical isolation, for example, by achieving a denser SiN_x layer or using another insulator, such as Al_2O_3 deposited by atomic layer deposition, could be used to fabricate an array with smaller interelectrode distances, thus increasing the redox cycling efficiency and producing lower LODs.

Selective Detection of DA in the Presence of AA. The integration of nanochannels with RRD arrays was shown above to enhance the measurement selectivity between a reversible analyte and an irreversible interference. Detection of DA in the presence of AA is challenged by the additional difficulty that there is strong overlap of the redox waves. Electrochemical oxidation[12,13,35,37] has been successfully used to deplete AA and reduce its interference on the electrochemical determination of other oxidizable species. Typically one electrode is set at a potential anodic of the oxidation potential of AA, allowing it to be eliminated before diffusing to the other electrode and interfering with the measurement. In the present experiments, this concept is extended by depleting AA inside a nanochannel via oxidation at the ring electrodes held at +0.5 V, while DA is detected at the disk electrodes.

Figure 4 shows a comparison of the CV results for a mixture of 0.1 mM DA and AA in the range of 0−10 mM for RRD

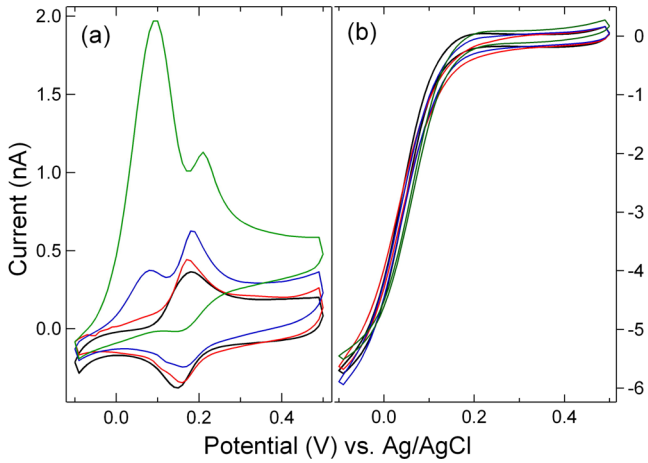

Figure 4. CV responses for dopamine (0.1 mM) in the presence of ascorbic acid with concentrations of 0 mM (black), 1.0 mM (red), 2.0 mM (blue), and 10 mM (green). Voltammograms were measured on a 25 μm × 50 μm RRD array by scanning the disk electrodes at 10 mV/s and either (a) floating the ring electrodes, non-GC mode, or (b) holding them at +0.5 V vs Ag/AgCl, GC mode.

arrays operated in GC, Figure 4b, and non-GC, Figure 4a, modes. Peak-shaped CVs were observed in both the cathodic and anodic scans when the experiments were performed in non-GC mode. The anodic current consists of two strongly overlapping peaks at ~0.08 and ~0.18 V, which are attributed to the oxidation of AA and DA, respectively, while the cathodic current is composed of only a single peak at ~0.15 V, which is attributed to the reduction of DA. As expected, the CV response obtained in non-GC mode depends strongly on the concentration of AA, making accurate measurements of DA currents at 100-fold AA excess (green curve, Figure 4a) extremely difficult. In contrast, when the experiments are run in GC mode, and the ring electrodes are held at +0.5 V, the steady-state currents observed at the disk electrodes are clearly independent of the concentration of AA, Figure 4b. This is likely due to the AA being oxidized at the ring electrodes before diffusing to the disk electrode, as confirmed by the absence of oxidation current at the disk electrodes. It is clear that the depletion of AA decreases the current associated with AA at the disk electrode, eliminating its interference in the measurement of DA. The selectivity of DA versus AA at the disk is ~2700 compared to the selectivity of ~70 in Figure 2b for the case of $Ru(NH_3)_6^{2/3+}$ in the presence of AA. In addition, the small variance (<5%) in the limiting current of DA demonstrates the capability of the RRD array to render high-precision interference-free measurements in the presence of 100-fold higher concentrations of AA.

Analytes with Similar Redox Reversibility and Resolved Electrochemical Waves. Aside from its ability to

dx.doi.org/10.1021/ac402417w | Anal. Chem. 2013, 85, 9882−9888

improve selectivity based on redox reversibility, the RC effect can also differentiate species with similar redox reversibility based on differences in redox potential. Through proper control of the generator and collector potential, interfering species can be forced to exhibit exclusively cathodic(anodic) current at the collector electrode,[3,48] thus allowing the target to be determined from the corresponding anodic(cathodic) current, at the same electrode. In order to elucidate the mechanism and explore the capability of the array for selective detection, species with similar redox reversibility and different degrees of overlapping potential were investigated.

Figure 5 shows a comparison of CVs for a mixture of $Ru(NH_3)_6^{3+}$ and $Fe(CN)_6^{3-}$ measured at the disk electrodes of

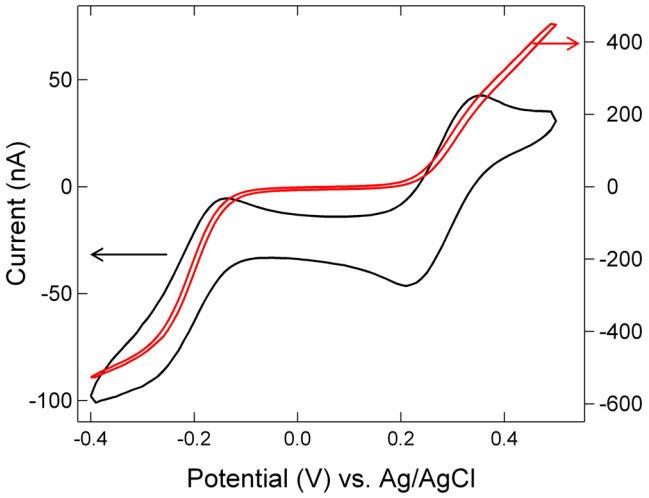

Figure 5. Cyclic voltammograms measured in a mixture of 1 mM $Ru(NH_3)_6^{3+}$ and 1 mM $Fe(CN)_6^{3-}$ on a 100 μm × 200 μm RRD array. Disk electrodes are swept at 100 mV/s. Ring electrodes are disconnected (black, left *Y*-axis) or held at +0.1 V vs Ag/AgCl (red, right *Y*-axis).

an RRD array, while the ring electrodes are either floating or held at +0.1 V. With the ring electrodes disconnected both species exhibit peak-shaped responses with sufficient separation to extract the current from each species by baseline subtraction, a procedure in which the capacitive current must be measured and corrected. However, by holding the rings at +0.1 V, the current at the disk can easily be distinguished as two steady-state responses that are well-separated in potential. The cathodic and anodic parts of the GC mode response (red curve, Figure 5) correspond to the response of $Ru(NH_3)_6^{3+}$ and $Fe(CN)_6^{4-}$, respectively. The availability of each species in the appropriate region of the voltammogram is attributed to the modulation of the reactions at the disk electrodes by the potential of the rings.[3,48] The species that diffuse to the disk electrodes are exclusively $Ru(NH_3)_6^{3+}$ and $Fe(CN)_6^{4-}$ when the ring electrodes are held at +0.1 V, in the plateau region of the GC mode response. In addition, Figure 5 clearly shows that GC mode greatly enhances the faradic current relative to the charging current, as typically observed in redox cycling.

Analytes with Similar Redox Reversibility and Overlapping Electrochemical Waves. RRD arrays may also be applied to address the redox behavior of species that have overlapping electrochemical waves. Figure 6 shows the CV of a mixture of $Fe(CN)_6^{3-}$ and DA at pH 2. An acidic solution was employed to avoid strongly overlapping voltammograms of DA and $Fe(CN)_6^{3/4-}$ by taking advantage of the pH dependence of

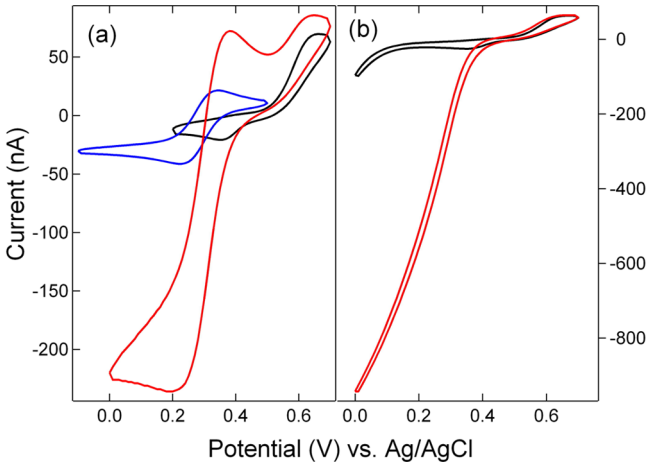

Figure 6. (a) Cyclic voltammograms with ring electrodes floating in 1 mM dopamine (black), 1 mM $Fe(CN)_6^{3-}$ (blue), or a mixture of 1 mM dopamine and 5 mM $Fe(CN)_6^{3-}$ (red) at a 100 μm × 200 μm RRD array. (b) Cyclic voltammograms with ring electrodes at +0.5 V vs Ag/AgCl in 1 mM dopamine (black) or a mixture of 1 mM dopamine and 5 mM $Fe(CN)_6^{3-}$ (red) at a 100 μm × 200 μm RRD array. Disk electrodes are swept at 100 mV/s, dopamine-containing solutions at pH 2 in both panels.

the DA oxidation potential. It is not possible to select a ring potential to make the two species exhibit exclusively anodic/cathodic behavior as in the case of $Ru(NH_3)_6^{2/3+}$ and $Fe(CN)_6^{3/4-}$. However, at a ring potential E_{ring} = +0.5 V the interference, $Fe(CN)_6^{3/4-}$ (not shown), exhibits only a cathodic current, while the analyte, DA, exhibits both anodic and cathodic currents, as shown in Figure 6b. The dopamine can then be determined from its anodic current. The presence of a 5-fold excess of $Fe(CN)_6^{3-}$ changes the anodic response of DA by <3%, thus allowing the accurate determination of DA in the presence of an excess of the interfering species.

These results clearly demonstrate the ability of the RRD array to differentiate species with overlapping CVs using GC mode and the RC effect. The ultimate limit of these capabilities addresses species with strongly overlapping voltammograms, such as those for ferrocenemethanol and $Fe(CN)_6^{3/4-}$ at low analyte concentration, and is illustrated in Figure 7. By holding the ring potential at +0.18 V, ferrocenemethanol can be determined from its cathodic current on the disks or anodic current on the rings in the presence of a 5-fold excess $Fe(CN)_6^{4-}$ with <10% deviation. While a similar selectivity enhancement was observed on both disk and ring electrodes, the ring electrodes, held at constant potential, show much smaller charging current, demonstrating the capability of the device for differentiating species at a lower concentration (approximately micromolar). In addition, the results of Figures 6 and 7 show that, using the proper combination of ring potential and sweep parameters, current from the analyte can be accurately measured in the presence of an excess of the interfering species, even when it has similar redox reversibility and overlapping redox potential. The separation achieved is a direct result of the redox cycling available in GC mode coupled with efficient conversion of interferences in the nanoscale RRD geometry.

■ CONCLUSIONS

The work presented here illustrates that recessed ring−disk electrode arrays with nanometer-scale interelectrode spacing

dx.doi.org/10.1021/ac402417w | *Anal. Chem.* 2013, 85, 9882−9888

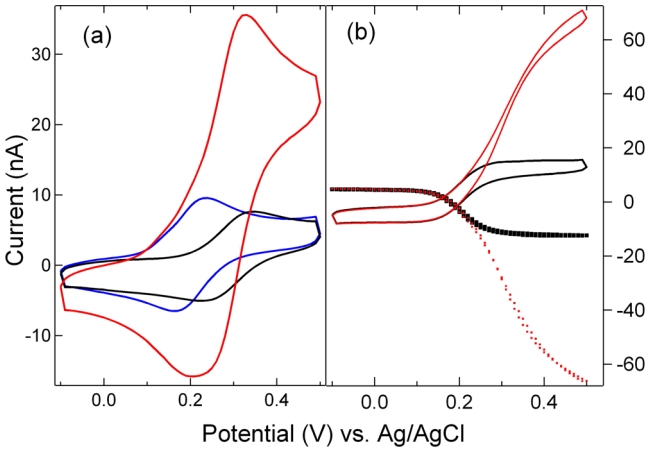

Figure 7. (a) Cyclic voltammograms with ring electrodes floating in 0.1 mM ferrocenemethanol (black), 0.1 mM $Fe(CN)_6^{4-}$ (blue), or a mixture of 0.1 mM ferrocenemethanol and 0.5 mM $Fe(CN)_6^{4-}$ (red) using a 100 μm × 200 μm RRD array. (b) Cyclic voltammograms with ring electrodes held at +0.18 V vs Ag/AgCl in 0.01 mM ferrocenemethanol (black) or a mixture of 0.01 mM ferrocenemethanol and 0.05 mM $Fe(CN)_6^{4-}$ (red) using a 100 μm × 200 μm RRD array. Disk electrodes are swept at 100 mV/s. Disk current (solid) and ring current (dashed).

and their incorporation within nanochannels can be employed for selective detection of electroactive species in the presence of significant interference. The combination of redox cycling enabled by the RRD array and interference depletion resulting from confinement of the array within a nanochannel is important. This is evidenced by the improvement of selectivity for $Ru(NH_3)_6^{3+}$ in the presence of ascorbic acid from a value of 10 for the RRD array in an open geometry to 70 when the array is confined to a nanochannel. Measured selectivity for dopamine in the presence of ascorbic acid in the same configuration is 2700, allowing detection of dopamine in the presence of large excesses of ascorbic acid. Furthermore, nanoscale RRD arrays can efficiently separate redox processes in which the interfering species is electrochemically reversible. By modulating the reaction at the disk electrodes with the ring potential, the array is capable of differentiating an analyte response in the presence of a reversible interfering species, even when the interference has strongly overlapping CV response. Thus, careful design of electrochemical assays can enable analysis of mixtures when preseparation is not desirable or possible.

AUTHOR INFORMATION

Corresponding Author

*E-mail: pbohn@nd.edu.

Notes

The authors declare no competing financial interest.

ACKNOWLEDGMENTS

This work was supported by the National Science Foundation Grant 1111739 (C.M.), NSF Grant 0852741 (L.R.G.), and the Department of Energy Basic Energy Sciences Grant DE FG02 07ER15851 (N.M.C.). Fabrication and structural characterization of the devices studied here were accomplished at the Notre Dame Nanofabrication Facility and the Notre Dame Integrated Imaging Facility whose generous support is gratefully acknowledged.

REFERENCES

(1) Rossier, J. S.; Roberts, M. A.; Ferrigno, R.; Girault, H. H. *Anal. Chem.* **1999**, *71*, 4294−4299.
(2) Chabinyc, M. L.; Chiu, D. T.; McDonald, J. C.; Stroock, A. D.; Christian, J. F.; Karger, A. M.; Whitesides, G. M. *Anal. Chem.* **2001**, *73*, 4491−4498.
(3) Ma, C.; Contento, N. M.; Gibson, L. R., II; Bohn, P. W. *ACS Nano* **2013**, *7*, 5483−5490.
(4) Zen, J.-M.; Chen, P.-J. *Anal. Chem.* **1997**, *69*, 5087−5093.
(5) Rossier, J. S.; Girault, H. H. *Lab Chip* **2001**, *1*, 153−157.
(6) Goral, V. N.; Zaytseva, N. V.; Baeumner, A. J. *Lab Chip* **2006**, *6*, 414−421.
(7) Chikkaveeraiah, B. V.; Liu, H.; Mani, V.; Papadimitrakopoulos, F.; Rusling, J. F. *Electrochem. Commun.* **2009**, *11*, 1092.
(8) Huang, C.-J.; Chien, H.-C.; Chou, T.-C.; Lee, G.-B. *Microfluid. Nanofluid.* **2011**, *10*, 37−45.
(9) Figeys, D.; Pino, D. *Anal. Chem.* **2000**, *72*, 330A−335A.
(10) Xu, J.-J.; Bao, N.; Xia, X.-H.; Peng, Y.; Chen, H.-Y. *Anal. Chem.* **2004**, *76*, 6902−6907.
(11) Li, H.; Wu, N. *Nanotechnology* **2008**, *19*, 275301/1−275301/6.
(12) Wolfrum, B.; Zevenbergen, M.; Lemay, S. *Anal. Chem.* **2008**, *80*, 972−977.
(13) Goluch, E. D.; Wolfrum, B.; Singh, P. S.; Zevenbergen, M. A. G.; Lemay, S. G. *Anal. Bioanal. Chem.* **2009**, *394*, 447−456.
(14) Figeys, D.; Gygi, S. P.; McKinnon, G.; Aebersold, R. *Anal. Chem.* **1998**, *70*, 3728−3734.
(15) Brivio, M.; Fokkens, R. H.; Verboom, W.; Reinhoudt, D. N.; Tas, N. R.; Goedbloed, M.; van den Berg, A. *Anal. Chem.* **2002**, *74*, 3972−3976.
(16) Dethy, J.-M.; Ackermann, B. L.; Delatour, C.; Henion, J. D.; Schultz, G. A. *Anal. Chem.* **2003**, *75*, 805−811.
(17) Contento, N. M.; Branagan, S. P.; Bohn, P. W. *Lab Chip* **2011**, *11*, 3634−3641.
(18) Pais, A.; Banerjee, A.; Klotzkin, D.; Papautsky, I. *Lab Chip* **2008**, *8*, 794−800.
(19) Hayashi, K.; Iwasaki, Y.; Horiuchi, T.; Sunagawa, K.; Tate, A. *Anal. Chem.* **2005**, *77*, 5236−5242.
(20) Wang, J. *Talanta* **2002**, *56*, 223−231.
(21) Baldwin, R. P.; Roussel, T. J., Jr.; Crain, M. M.; Bathlagunda, V.; Jackson, D. J.; Gullapalli, J.; Conklin, J. A.; Pai, R.; Naber, J. F.; Walsh, K. M.; Keynton, R. S. *Anal. Chem.* **2002**, *74*, 3690−3697.
(22) Chen, C.; Hahn, J. H. *Anal. Chem.* **2007**, *79*, 7182−7186.
(23) Menon, V. P.; Martin, C. R. *Anal. Chem.* **1995**, *67*, 1920−1928.
(24) Sandison, M. E.; Cooper, J. M. *Lab Chip* **2006**, *6*, 1020−1025.
(25) Guo, J.; Lindner, E. *Anal. Chem.* **2009**, *81*, 130−138.
(26) Lewis, P. M.; Sheridan, L. B.; Gawley, R. E.; Fritsch, I. *Anal. Chem.* **2010**, *82*, 1659−1668.
(27) Wang, Y.; Luo, J.; Chen, H.; He, Q.; Gan, N.; Li, T. *Anal. Chim. Acta* **2008**, *625*, 180−187.
(28) Illa, X.; Ordeig, O.; Snakenborg, D.; Romano-Rodriguez, A.; Compton, R. G.; Kutter, J. P. *Lab Chip* **2010**, *10*, 1254−1261.
(29) Branagan, S. P.; Contento, N. M.; Bohn, P. W. *J. Am. Chem. Soc.* **2012**, *134*, 8617−8624.
(30) Gibson, L. R., II; Branagan, S. P.; Bohn, P. W. *Small* **2013**, *9*, 90−97.
(31) Forry, S. P.; Murray, J. R.; Heien, M. L. A. V.; Locascio, L. E.; Wightman, R. M. *Anal. Chem.* **2004**, *76*, 4945−4950.
(32) Niwa, O.; Morita, M.; Tabei, H. *Anal. Chem.* **1990**, *62*, 447−452.
(33) Menshykau, D.; O'Mahony, A. M.; del Campo, F. J.; Munoz, F. X.; Compton, R. G. *Anal. Chem.* **2009**, *81*, 9372−9382.
(34) Vandaveer, W. R. I. V.; Woodward, D. J.; Fritsch, I. *Electrochim. Acta* **2003**, *48*, 3341−3348.
(35) Paixao, T. R. L. C.; Richter, E. M.; Brito-Neto, J. G. A.; Bertotti, M. *Electrochem. Commun.* **2006**, *8*, 9−14.
(36) Dam, V. A. T.; Olthuis, W.; van den Berg, A. *Analyst* **2007**, *132*, 365−370.
(37) Zhu, F.; Yan, J.-W.; Lu, M.; Zhou, Y.-L.; Yang, Y.; Mao, B.-W. *Electrochim. Acta* **2011**, *56*, 8101−8107.

(38) Niwa, O.; Tabei, H. *Anal. Chem.* **1994**, *66*, 285−289.
(39) Aggarwal, A.; Hu, M.; Fritsch, I. *Anal. Bioanal. Chem.* **2013**, *405*, 3859−3869.
(40) Katelhon, E.; Hofmann, B.; Lemay, S. G.; Zevenbergen, M. A. G.; Offenhausser, A.; Wolfrum, B. *Anal. Chem.* **2010**, *82*, 8502−8509.
(41) Yu, S.; Luo, C.; Wang, L.; Peng, H.; Zhu, Z. *Analyst* **2013**, *138*, 1149−1155.
(42) Mo, J.-W.; Ogorevc, B. *Anal. Chem.* **2001**, *73*, 1196−1202.
(43) Venton, B. J.; Wightman, R. M. *Anal. Chem.* **2003**, *75*, 414A−421A.
(44) Gilbert, O.; Kumara, S. B. E.; Chandra, U.; Sherigara, B. S. *J. Electroanal. Chem.* **2009**, *636*, 80−85.
(45) Odijk, M.; Olthuis, W.; Dam, V. A. T.; van den Berg, A. *Electroanalysis* **2008**, *20*, 463−468.
(46) Oleinick, A.; Zhu, F.; Yan, J.; Mao, B.; Svir, I.; Amatore, C. *ChemPhysChem* **2013**, *14*, 1887−1898.
(47) Eddings, M. A.; Johnson, M. A.; Gale, B. K. *J. Micromech. Microeng.* **2008**, *18*, 067001.
(48) Zevenbergen, M. A. G.; Wolfrum, B. L.; Goluch, E. D.; Singh, P. S.; Lemay, S. G. *J. Am. Chem. Soc.* **2009**, *131*, 11471−11477.